



Synthesis and characterization of sustainable Zn(II) and ZnO/chitosan Schiff base hydrogel for antimicrobial application

Marwa M. Abd El-Hady^{a*}, Fahad M. Alminderej^a, Abuzar E. A. E. Albadri^a,
and Saeed El-Sayed Saeed^a

^a Department of Chemistry, College of Science, Qassim University, Saudi Arabia



Abstract

A significant amount of interest in Schiff bases (SBs) produced from metal-based hydrogels and chitosan has recently been garnered for their biological applications. We successfully synthesised a new hydrogel by crosslinking chitosan with 2,3,4-trihydroxybenzaldehyde (THB) to produce chitosan Schiff base (CSB) and subsequently created its Zn(II) metal composite and ZnO nanoparticles. Two different concentrations of Zn(II) ions (1% w/v and 1.5% w/v) and mass ratio of (CS: THB) of 1.0:0.25, 1.0:0.5, 1.0:1.0 and 1.0: 1.5 were studied. The structure and characteristics of the composite hydrogels are characterised using various techniques. The synthesised CSB and its nanocomposites were confirmed using XRD analysis, UV–Vis spectroscopy, and FTIR. The interactions among chitosan and metals, thermal stability, surface shape, and the elemental presence of metal ions in the hydrogels were analysed using FTIR, TGA, SEM, NMR, and EDX techniques. The synthesized CSB hydrogels were tested for their swelling manners at different temperatures (30, 45, and 60 °C) and pH (4, 7, 10). The antimicrobial applications were also investigated. The results indicate that the most significant degree of swelling occurs at low pH levels. The ZnO@CSB nanocomposite hydrogel has a swelling degree of 267%, whereas the Zn(II)@CSB nanocomposite hydrogel has a swelling degree of 260%. The antimicrobial tests demonstrated that all hydrogels and their nanocomposites possess potential antimicrobial activity against *Staphylococcus aureus*, *Escherichia coli*, and *Candida albicans*. From the results, all samples demonstrate higher antimicrobial activity against *Candida albicans* than against bacterial strains. The ZnO@CSB nanocomposite hydrogel exhibited the maximum inhibition rate at 19 mm, compared with the Zn(II)@CSB nanocomposite hydrogel at 15 mm. Furthermore, the hydrogel that was synthesized displayed significant values of tensile strength as well as elongation at break. Finally, these innovative hydrogels can be promising candidates for sustainable biomedical applications and wound dressing materials.

Keywords: Hydrogel; Chitosan; Schiff bases; Antimicrobial activity; Nanocomposite; Mechanical properties

1. Introduction

Hydrogel compounds can absorb a significant amount of water and swell without disintegrating in aqueous environments. Under aqueous conditions, hydrogel compounds can absorb a significant amount of water and expand without disintegrating. The three-dimensional crosslinked network of hydrophilic polymer chains is responsible for the distinctive performance characteristics of hydrogels. Hydrogels have recently garnered significant attention due to their potential applications in a wide range of biomedical fields, including tissue engineering and controlled drug delivery systems. Hydrogels can provide 3D microenvironments that encourage cell migration, adhesion, and proliferation while also facilitating the flow of nutrients and signalling chemicals. This is because they can mimic the biomechanical properties of the native extracellular matrix (ECM). Additionally, due to their hydrophilic nature, high swelling ability, and porosity, hydrogels are well-suited for carrying hydrophilic biologically active substances, including medicines, biomolecules, and phytochemicals. Generally, the degree of crosslinking has a significant impact on all these hydrogel characteristics [1,2].

Chitosan's (CS) antimicrobial and adsorbent properties, as well as its high hydrophilicity, biocompatibility, and biodegradability, have garnered considerable attention [3]. Chitin deacetylates to CS [4]. The second most common polymer in nature, after cellulose, is chitin [5]. From the shells of crustaceans, such as prawns and crabs, as well as fungi, insects, and various types of shellfish, it can be extracted [6]. The fundamental structural unit of chitosan (CS), a natural biodegradable polymer, is 2-amino-2-deoxy-d-glucopyranose, and the units are linked together by 1,4-glycosidic linkages [7]. Its abundance of amino and hydroxyl groups makes it suitable as a natural adsorbent for pollution removal [8]. Anti-microbial activity is one of chitosan's most important bioactive properties. It has been demonstrated to be effective against a range of bacteria, including both Gram-positive and Gram-negative species [9]. Furthermore, CS has several advantages over other antimicrobial medicines, including better antibacterial activity, a wider range of action, a lower mortality rate, and reduced toxicity to mammalian cells [10]. However, the use of chitosan in adsorption applications and antimicrobial activity has been limited due to its high index of swelling, low mechanical strength, chemical instability in acidic environments, and small surface area [11]. To address these challenges and improve the properties and applications of chitosan, various processes have been employed, including functionalization with organic groups [12], grafting with carbon materials, blending with inorganic

*Corresponding author e-mail: m.aish@qu.edu.sa; (Marwa M. Abd El-Hady)

Receive Date: 23 February 2025, Revise Date: 24 March 2025, Accept Date: 09 April 2025

DOI: 10.21608/ejchem.2025.361527.11348

©2025 National Information and Documentation Center (NIDOC)

materials [13], and the production of nanocomposites [14]. Attempts to modify chitosan through a Schiff base (SB) reaction have recently been extended [15], as they can be employed in various applications, including antibacterial activity [16], anticancer activity, and the removal of hazardous dyes from aqueous media. Previous research has demonstrated that phenolic chitosan SB exhibits greater antibacterial and anticancer activity compared to unmodified chitosan. Iminic groups commonly promote biological functions [16]. In recent years, considerable research has been conducted on the development of chitosan-based hydrogels [17,18]. Hydrogels can be prepared by physically and chemically bonding various types of cross-linkers to the NH_2 and OH groups of chitosan (CS). The dynamic behaviour of the hydrogels produced may be attributed to the NH_2 groups of CS, which enable this carbohydrate to form SB bonds with aldehydic compounds [19, 20]. The simplicity, reversibility, pH sensitivity, and biocompatibility of SB linkages, which include imine groups, confer upon them great thermal stability and promise future applications in biomedicine [21]. Hydrogels like these are also reversible, sensitive to disruption under specific conditions, and responsive to chemical conditions such as pH [22, 23]. Previous studies have demonstrated the use of chitosan Schiff base hydrogels for various applications. Abdalla, T. H. et al. prepared different chitosan Schiff base hydrogels using various crosslinking agents and utilized them in wastewater treatment [24]. Xu, C. et al., used aniline as a natural aldehyde for crosslinking and designed a self-healing hydrogel [25]. Recently, Heydari, N. et al., chitosan-based hydrogel sunscreens modified by 2,4-dihydroxybenzaldehyde and vanillin as UV absorbers and cross-linkers. The prepared hydrogel has antioxidant, UV protection, and self-healing properties [26].

Inorganic nanocomposite hydrogels have garnered significant interest among antibacterial hydrogels [27]. Nonetheless, the toxicity resulting from the accumulation of silver or gold-based compounds in the human body is a significant challenge [28]. Zinc oxide nanoparticles (ZnO NPs) are recognised for their antimicrobial properties and have been utilised in cosmetic products and food packaging. The safety of ZnO is approved by the U.S. Food and Drug Administration (FDA). The antimicrobial properties of 2,3,4-trihydroxybenzaldehyde (THB) have garnered some attention [29]. Additionally, the presence of aromatic -OH and aldehydic groups in THB enables the formation of a series of one-pot, physically synthesised hydrogels with various polymers [30]. The aim of this work is to develop a modified nanocomposite chitosan hydrogel based on Schiff base preparation. Herein, we first designed a fast crosslinking hydrogel (CSB) through a Schiff base reaction between a chitosan compound and 2,3,4-trihydroxybenzaldehyde (THB) in different ratios. Second, enhancer Zn(II) and in situ prepared ZnO nanoparticles were introduced during the preparation of the CSB hydrogel to improve its properties. Various characterisation methods were employed to study the morphological, chemical, thermal, and mechanical properties of hydrogels. In addition, the swelling degree of the prepared hydrogels at different pH was evaluated. Finally, the antimicrobial activity leading to design a hydrogel for medical application.

2. Experimental

2.1 Chemicals

Chitosan (CS) high molecular weight, deacetylation degree > 75%, acetic acid, methyl alcohol, NaOH, 2,3,4-trihydroxy benzaldehyde, hydrochloric acid and zinc nitrate were supplied by Sigma-Aldrich and were used as received. Buffer solutions at 4, 7, and 10 were used. All chemicals were used as received without any purification.

2.2 Preparation of chitosan Schiff base hydrogel (CSB)

To prepare CS, 1% (w/v), 0.25 g of chitosan was dissolved in 1% glacial CH_3COOH solution (25 ml), stirring at room temperature for half hr. until the solution became transparent. The series of crosslinking (THB) solutions were prepared by dissolving 0.25, 0.50, 1.0 or 1.5 g of THB in 5 mL of methyl alcohol, respectively. Next, hydrogels with mass ratios (CS: THB) of 1.0:0.25, 1.0:0.5, 1.0:1.0, and 1.0:1.5 were prepared by adding the THB solution to a 25 mL 1% (w/v) CS solution. Thereafter, the mixture was stirred at 30 °C until gelation was achieved. Additionally, the gelation times at 45 °C and 60 °C were studied. The hydrogels that had been produced were poured into petri dishes and dried at 50 °C for 24 hours.

2.3 Preparation of Zn (II) @ CSB nanocomposite hydrogel

The prepared optimum concentration of CSB solutions (1:0.5) was mixed for 1 hour at 45 °C with 10 ml solutions of $\text{Zn}(\text{NO}_3)_2$ of different concentrations 1 % (w/v) and 1.5% (w/v). The polymer was cross-linked by the formation of composite between the nitrogen atom of the imine group and the hydroxyl group of THB and the Zn metal ions. The nanocomposite hydrogels that were synthesized were subsequently poured into petri dishes and desiccated at 50 °C for 24 hours.

2.4 Preparation of ZnO@CSB nanocomposite hydrogel

The concentration of $\text{Zn}(\text{NO}_3)_2$ was 0.2 g in 25 mL of distilled H_2O , which was dissolved by stirring for 30 minutes. The previous solution was stirred for an additional 1 hour at 45 °C after the addition of 0.2 g of the previously prepared CSB hydrogel. Then, a 0.2 M NaOH solution was added to the solution in a dropwise manner until a faintly brownish yellow hydrogel was obtained. The reaction was then allowed to stir for an additional 30 minutes. The nanocomposite hydrogels that were synthesized were subsequently poured into petri dishes and desiccated at 50 °C for 24 hours.

2.5 Instruments

The prepared samples were subjected to ^1H NMR spectroscopy at 850 MHz using a Bruker spectrometer (MA, USA) with deuterated DMSO as the solvent. The Agilent spectrometer (Cary 600 FTIR, USA) was employed to measure the FTIR spectra of CSB and its composite hydrogels, with a wavenumber range of 4,000–400 cm^{-1} . A Shimadzu UV-Vis spectrophotometer (UV-1650PC, Japan) was used to quantify DMSO solutions (1×10^{-3} M) of CSB and its composites. The Shimadzu simultaneous TG apparatus (DTG-60AH, Japan) was used in the air at a heating rate of 10 °C/min, with a temperature range of room temperature to 700 °C. The samples' XRD patterns were measured using $\text{Cu K}\alpha$ radiation ($\lambda = 1.54180 \text{ \AA}$) on a Rigaku Ultima IV XRD diffractometer (USA). The JEOL-JEM-1230 transmission electron microscopy (TEM) (with an accelerating voltage range of 40–120 kV) and scanning electron microscopy (SEM) (Tescan Vega3) with an attached energy-dispersive X-ray spectrometer (EDX) were employed for the electron microscopy investigations. To make the

samples electron-conductive, SEM samples were prepared on a suitable disk and coated with gold. The mechanical properties of the hydrogels were evaluated following ASTM D412 using an electronic universal tensile testing machine (ZQ990, Dongguan, China).

2.6 Swelling properties of hydrogels

The swelling degree of the hydrogels prepared was evaluated by soaking 0.1 g of dry hydrogel in 50 mL of medium at room temperature. The extent of hydrogel swelling in distilled water, acidic, and basic media was determined by adjusting the pH conditions using buffer solutions at pH 4, 7, and 10. Additionally, the weight of the distended hydrogel was measured at 5-minute intervals, followed by measurements at 10, 15, 20, and 25 minutes. Equation (1) was used to determine the equilibrium swelling degree.

$$\text{swelling degree (SD)} = \frac{W_s - W_d}{W_d} \times 100 \quad \text{Eq. 1}$$

Where W_d represents the dried hydrogel weight in grams, and W_s represents the swollen hydrogel weight in grams.

2.7 Antibacterial test

The agar diffusion test was conducted per the qualitative methodology to assess the antimicrobial activity of the prepared CSB hydrogel and its composite samples [31].

2.8 Statistical analysis

The experimental data in this investigation were presented as the mean \pm standard deviation. The swelling study presented in this study was conducted three times, and the average values were considered. Error bars were all calculated by using 2016 Microsoft Excel.

3. Results and discussion

3.1 Synthesis of CSB hydrogel

The fabrication of a chitosan Schiff base (CSB) crosslinked hydrogel was effectively achieved by employing 2,3,4-trihydroxybenzaldehyde (THB) as the crosslinking agent, which possesses an aldehyde reactive group (Fig. 1). This crosslinker facilitates the development of bonding between CS chains, resulting in a network structure. Additionally, the hydrogel is formed through intermolecular hydrogen bonding between the hydroxyl groups of THB and the hydroxyl and/or amino groups of the chitosan molecule, resulting in a more stable hydrogel. The hypothesized structure and reaction for the formation of the CSB hydrogel are depicted in step 1 of Fig. 1a.

This mechanism illustrates the crosslinking of the amino groups of chitosan with the CHO groups of THB. The nitrogen in the NH_2 of CS, which operates as a nucleophile, initially attacks the electrophilic carbonyl carbon of the aldehyde group within the THB structure. Subsequently, nitrogen undergoes deprotonation, causing the electrons from the N-H bond to reject the oxygen from carbon, resulting in the formation of a chemical (an imine) characterised by a -C=N double bond, referred to as a Schiff base, while displacing a water molecule [32,33]. Consequently, the crosslinked CS was effectively produced, as shown in step 2 in Fig. 1b, illustrating the incorporation of Zn (II) ion during hydrogel development. The Zn(II) ion indicates coordination via the N atom of the C=N group and the oxygen atom of the deprotonated hydroxyl group [34]. In Fig. 1b, the hydroxyl groups on the CSB may interact with the Zn ions in the solution. Under the alkaline conditions, Zn ions were oxidised to form ZnO nanoparticles.

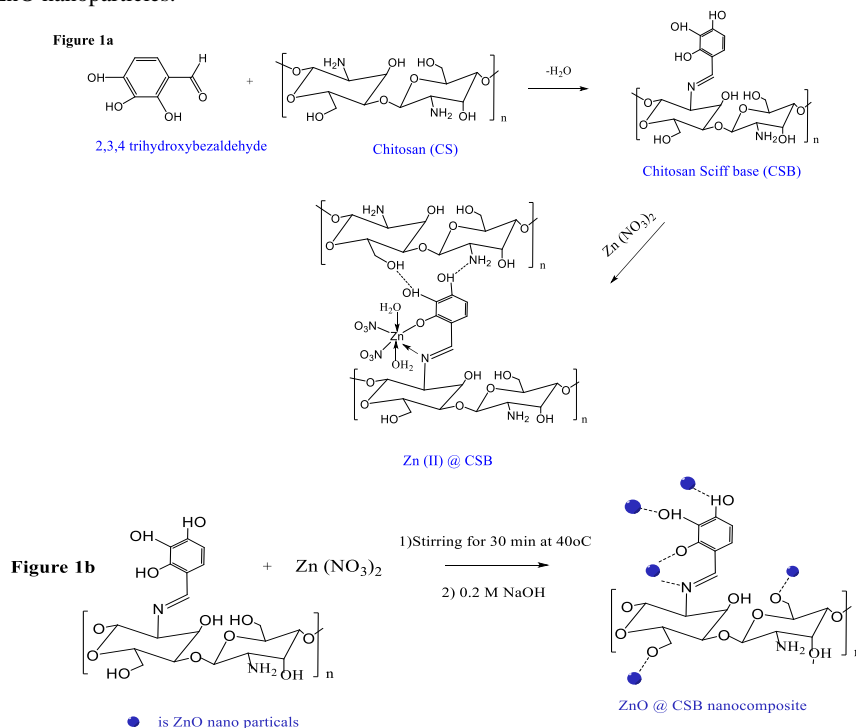


Figure 1. Schematic mechanism for preparation of hydrogels

3.2 Swelling Studies of CSB

Swelling is a fundamental characteristic of hydrogels and is often employed for preliminary assessment before thorough evaluation. This study illustrates that the water absorption of CSB hydrogel is affected by the synthesis conditions. The maximum swelling time was observed at 15 minutes. **Fig. 2** and **Fig. 3** illustrate the swelling study at different pH levels to observe the effects of THB as a crosslinker and reaction temperature, loading of Zn(II) ions, and loading of ZnO nanoparticles on the hydrogel swelling ratio. The amount of crosslinker has a strong effect on swelling ratio. The number of molecules that contribute to the formation of the CSB increases as the concentration of crosslinker increases. Furthermore, the gel's swelling decreased as THB increased. The water absorption of CSB hydrogel is high when the THB amount is comparatively small, as illustrated in **Fig. 2a** [35]. It is evident from **Fig. 2a** that the swelling ratio reaches its maximum value of 230% as the concentration of THB increases from 0.25% to 0.5%. Furthermore, as the concentration of THB increased further to 1.5%, the swelling ratio decreased. Increasing the crosslinker concentration results in a greater number of crosslinking sites and a reduction in free hydrophilic amino groups in CS, leading to a more compact structure. Thus, a hydrogel CSB with a higher crosslinking density keeps less H₂O than one with a lower CSB crosslinking density. At a cross-linker concentration of 0.5%, swelling capacity was significantly improved. The swelling degree of CSB hydrogel is affected by temperature, as illustrated in **Fig. 2b**. The swelling increases from 208% to 230% when the temperature is raised from 30°C to 45 °C. The higher temperatures enhance the diffusion rate of the solution into the CSB hydrogels and improve the capacity for absorbing; however, a further temperature rise subsequently decreases the swelling degree. This can be attributed to the rapid formation of Schiff-base crosslinks, which establish the entire network [36]. Consequently, the swelling ratio decreases. 0.5% THB and 45 °C are the optimal conditions for hydrogel preparation.

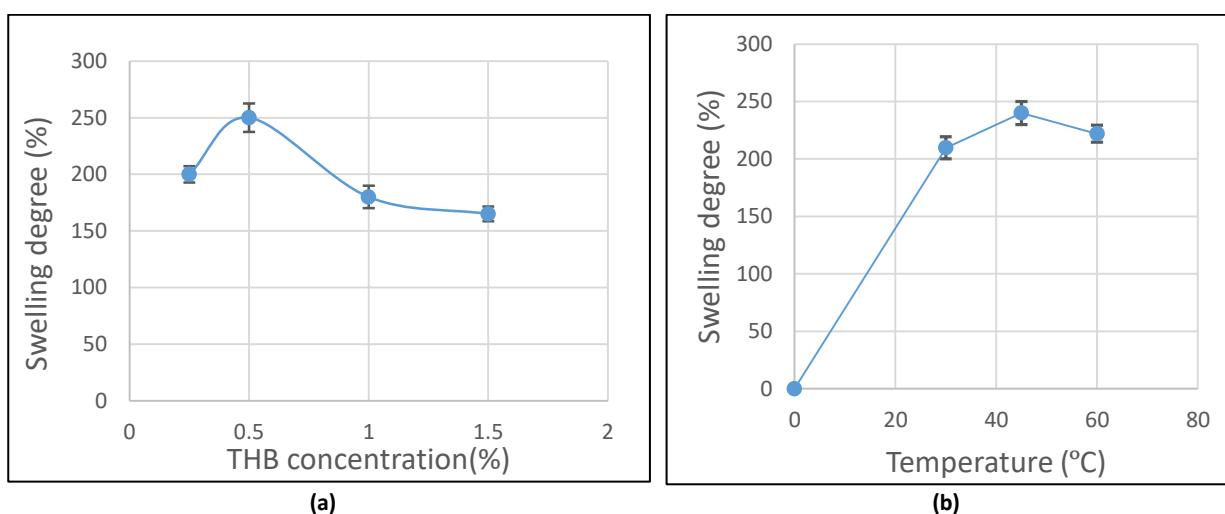


Figure 2. Effects of (a) THB concentration (b) temperature on swelling of CSB hydrogel

3.3 pH-effect on Swelling of CSB, Zn (II) @CSB and ZnO @CSB Nanocomposite Hydrogels

The swelling response of CSB hydrogels was examined at different pH levels (4, 7, and 10), as shown in **Fig. 3a**. The CSB hydrogels synthesised exhibited distinct swelling behaviours in acidic and basic pH solutions, as illustrated in this figure. The swelling ratio increased as the pH decreased. As shown in **Fig. 3a**, the highest swelling degree is observed at 15 min and at an acidity of pH 4, with a value of 250%. By increasing the pH to 7 and 10, the swelling degree decreases to 230% and 190%, respectively. The results may be attributable to the protonation of NH₂ groups of CS only at pH 4. As a result, the protonation of -NH₂ groups at low pH leads to the dissociation of secondary bonds and electrostatic repulsion among positive charges. This causes network expansion and increased water penetration into the hydrogel matrix. At elevated pH, the strengthening of H bonding interactions among CS chains, resulting from the deprotonation of -NH₂ groups, diminishes swelling [36]. **Fig. 3b** illustrates the impact of Zn (II) ion and ZnO nanoparticle loading on the swelling degree of CSB hydrogel at various pH levels. **Fig. 3b** indicates that the swelling degree increased by up to 260% after the introduction of Zn (II) ions at a concentration of 1% (w/v) in the developed hydrogel, while a further increase in Zn (II) ion concentration to 1.5% (w/v) resulted in an insignificant improvement in swelling value. Conversely, the incorporation of nano ZnO during the manufacture of CSB hydrogel increases the swelling degree to 267%. The incorporation of nano ZnO particles into the hydrogel structure results in the expansion of the hydrogel network, leading to the formation of pores and vacancies, thereby enhancing water absorption in the bio-nanocomposite structure [37,38].

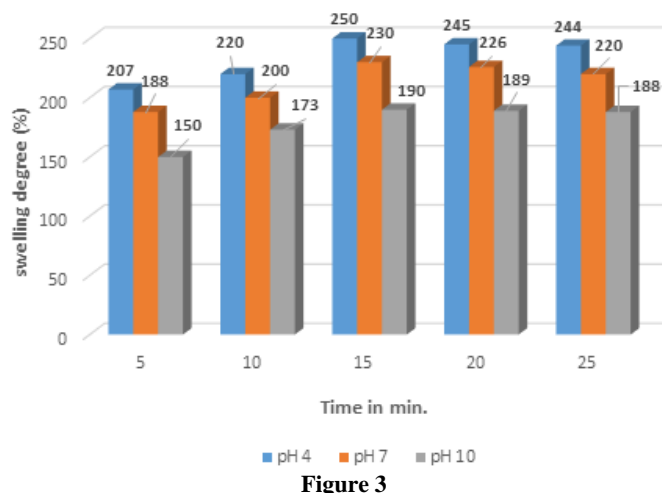


Figure 3

3.2 Characterization

3.2.1. NMR analysis

The ^1H NMR signals of the chitosan (deacetylation > 75%) and the prepared chitosan Schiff base (CSB) hydrogel were obtained, as shown in Fig. 4(a) and (b). The ^1H NMR signal in deuterated DMSO was used to investigate the CS-g-GEL hydrogel. As shown in Fig. 4a, the multiple peaks of chitosan at 1.98 to 3.64 ppm were assigned to H1, H3, H4, H5, and H6. The signals at 4.43 and 4.845 ppm are attributed to the anomeric proton of chitosan, specifically the H1 and H4 protons [39]. The NH_2 proton signal appeared at 4.85 ppm. The OH protons of chitosan have chemical shifts at 5.33 and 5.73 ppm. These signals disappeared in CSB NMR Fig. 4b, which may be due to hydrogen bonding with the hydroxy groups of the aromatic ring [40]; these values disappeared in CSB due to the formation of an H bond between some glucosamine units. The signal at 1.9 ppm is due to the presence of the CH_3 group of the N-acetyl residue [41]. The new signals appeared in the CSB signal in the signals area 6- 12 ppm due to the formation of the CSB and the aromatic moiety (Fig. 4b). The signal at 8.72 ppm is due to the proton of azomethine. The three OH protons of the aromatic ring appeared, H10, H11, and H12, appeared at 9.86, 10.6, and 11.99 ppm. The aromatic ring protons H8 and H9 appeared at 6.38-7.17 ppm. The observed peaks corresponding to various functional groups and the azomethine proton confirm the successful formation of CSB.

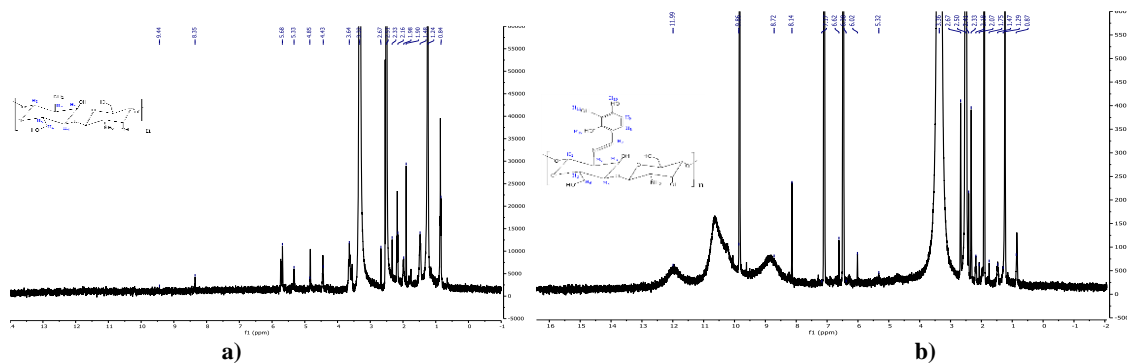


Figure 4: HNMR of a) Chitosan and b) CSB hydrogel

3.2.2. FTIR analysis

The FTIR spectra of chitosan, CSB hydrogel, $\text{Zn(II)}@$ CSB, and $\text{ZnO}@$ CSB nanocomposites are illustrated in Fig. 5a and 5b. In Fig. 5a, the chitosan spectrum exhibits stretching (ν) vibrations for $-\text{NH}_2$ and $-\text{OH}$ groups within the broadband range of $3550\text{--}3200\text{ cm}^{-1}$. The stretching (ν) peak of C-H is observed at 2862 cm^{-1} , with additional peaks at 1650 cm^{-1} and 1580 cm^{-1} corresponding to the amide groups and the symmetrical stretching (ν_s) vibration of NH_2 groups [42]. In Fig. 5b, the FTIR spectra of the crosslinked chitosan hydrogel CSB exhibited a pronounced new vibration peak associated with the imine group ($-\text{CH}=\text{N}-$) at 1621 cm^{-1} , confirming the creation of an imine bond between the NH_2 groups of CS and the aldehydic group of THB. The band broadening from 3000 to 3600 cm^{-1} indicates the presence of $-\text{NH}_2$ and $-\text{OH}$ functional groups in the hydrogel. Fig. 5c and 5d illustrate the loading of Zn(II) ions at varying concentrations within the hydrogel. The two curves exhibit almost identical peaks, with numerous shifts in the position and intensity of bands relative to the CSB hydrogel (Fig. 5b), indicating an enhancement in the binding process. The O-H and N-H peaks in the range of 3000 to 3600 cm^{-1} exhibit broadening and a considerable decrease in transmittance upon the introduction of Zn(II) ions, indicating the participation of specific O-H and N-H groups in binding to Zn(II) . The spectrum shifts for the $-\text{CH}=\text{N}-$ group occurred from 1621 cm^{-1} to 1608 cm^{-1} and 1610 cm^{-1} , respectively, following Zn(II) loading. In addition, it was found that an absorption peak at 774 cm^{-1}

was caused by the vibration modes of the coordinated water molecules [43]. **Fig. 5e** illustrates the FTIR spectrum of the ZnO @CSB nanocomposite hydrogel. In comparison to **Fig. 5b**, all bands corresponding to the stretching vibrations of $-\text{NH}_2$, $-\text{OH}$, and imine $-\text{CH}=\text{N}-$ groups in the CSB hydrogel were displaced to lower wavenumbers. Furthermore, pronounced absorption peaks for the imine group are observed in comparison to the Zn@CSB nanocomposite hydrogel (**Fig. 5c and d**). The appearance of new peaks at 1300 and 1305 in the case of 1% and 1.5% Zn @CSB is attributed to the coordinated nitrate group [44]. This confirms the successful establishment of strong interactions between functional groups in CSB and Zn (II) ions, as well as nano ZnO.

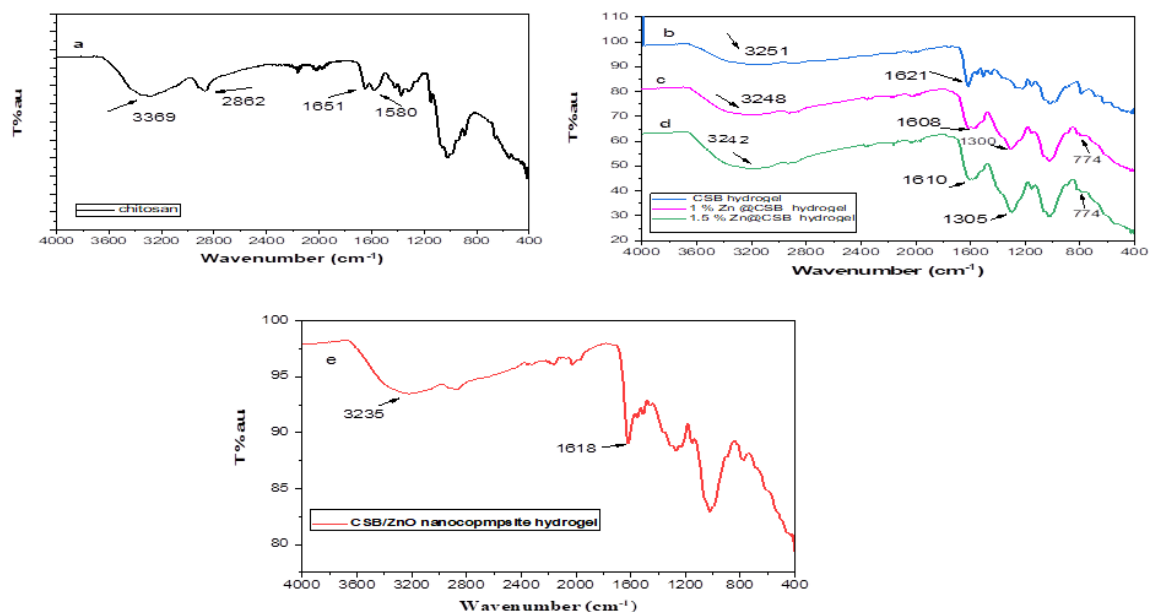


Figure 5 : FTIR of (a) chitosan, (b)CSB, (c) 1% Zn (II) @CSB, (d) 1.5% Zn (II) @CSB and , (e) ZnO @CSB nanocomposite hydrogels

3.2.3. XRD analysis

X-ray diffraction was utilised to provide a description of the structure and crystallinity of the hydrogels that were prepared. Through the use of X-ray diffraction, the structures of chitosan, CSB hydrogel, and its nanocomposite with zinc ions and zinc oxide nanoparticles were analyzed (**Fig. 6**). In **Fig. 6a**, the two primary peaks of chitosan (CS) are observed at approximately 2θ of 9.7° . Additionally, there is a prominent diffraction peak at 19.6° , which is attributed to stronger inter and intramolecular hydrogen bonding. This demonstrates that chitosan is a crystalline substance [45]. **Fig. 5b** demonstrates that the peak of chitosan, which was observed at a 2θ value of 9.7° , disappeared in the CSB hydrogel. In addition, the peak of CSB hydrogel, which was at 9.7° degrees, was not present. On the other hand, the 2θ of 19.6° degrees was shifted to 21.8° degrees, with a broader and less intense peak. This suggests that the structural changes in chitosan hydrogels are caused by the THC aldehydic substitution for forming azomethine ($\text{C}=\text{N}$) and the intermolecular interaction. **Fig. 6c and 5d** illustrate the Zn (II)@CSB nanocomposite hydrogel at varying concentrations: 1% Zn@ nanocomposite and 1.5 Zn @CSB nanocomposite, which exhibited the characteristic peak at 22.26° and 23.6° values of 2θ , respectively. The compound's crystal structure has been altered due to the formation of a composite between CSB hydrogel and Zn ions through $-\text{OH}$ and NH_2 binding sites, as evidenced by alterations in XRD patterns. The partials in nanometer scales were indicated by the broadening of the peaks [46]. On the other hand, the XRD peaks of the hydrogels performed a substantial shift when zinc oxide was incorporated into them. **Fig. 6e** illustrates that the experimental technique for synthesizing ZnO was feasible, as evident diffraction peaks were observed in the 2θ range of 12° – 50° , which follows the ZnO characteristic peaks [47].

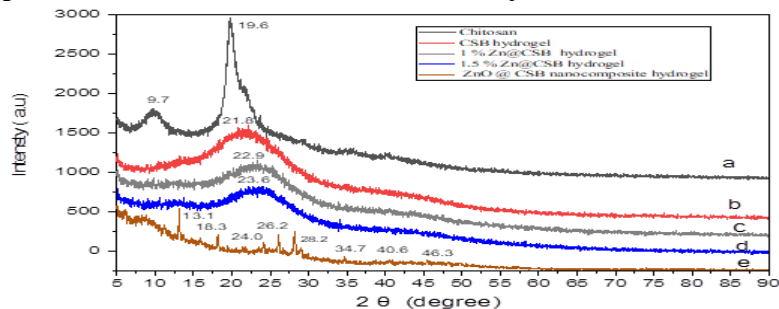


Figure 6: XRD of (a) chitosan, (b)CSB, (c) 1% Zn (II) @CSB, (d) 1.5% Zn (II) @CSB and , (e) ZnO @CSB nanocomposite hydrogels

3.2.4. SEM and EDX analysis

Scanning electron microscopy (SEM) was employed to study the morphology surface of hydrogels. The SEM images of chitosan, CSB hydrogel, Zn (II) @CSB nanocomposite hydrogel, and ZnO @CSB - nanocomposite hydrogel is depicted in Fig 7. The SEM images of chitosan in **Fig. 7a** indicate that it has a soft, compact, and homogeneous surface. Conversely, the SEM images of the prepared hydrogels exhibit a rough, surface-like morphology with a variety of lumps and pours, which indicates the successful preparation of hydrogels. The EDX analyses of CS, CSB hydrogel, Zn@CSB, and ZnO@CSB hydrogels are illustrated in Fig. 8. The EDX analysis reveals the elements present in the prepared hydrogels. The EDX spectrum of CS and CSB reveals the presence of C, N, and O (**Fig. 8a-b**). Conversely, the EDX spectrum of Zn @CSB and ZnO @CSB (**Fig. 8c-d**) clearly delineates the presence of the element zinc, as well as carbon, oxygen, and nitrogen. This suggests that the Zn ions and ZnO nanoparticles were successfully formed within the network of the prepared hydrogels.

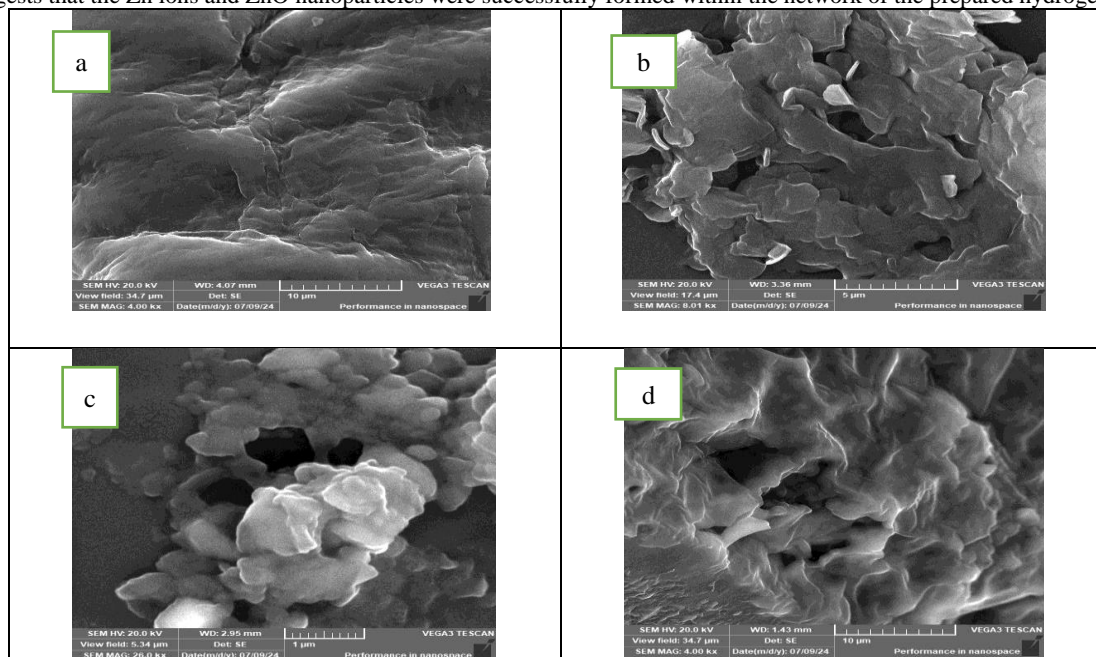


Figure 7: SEM images of (a) chitosan, (b) CSB, (c) Zn (II) @CSB and, (d) ZnO @CSB nanocomposite hydrogels

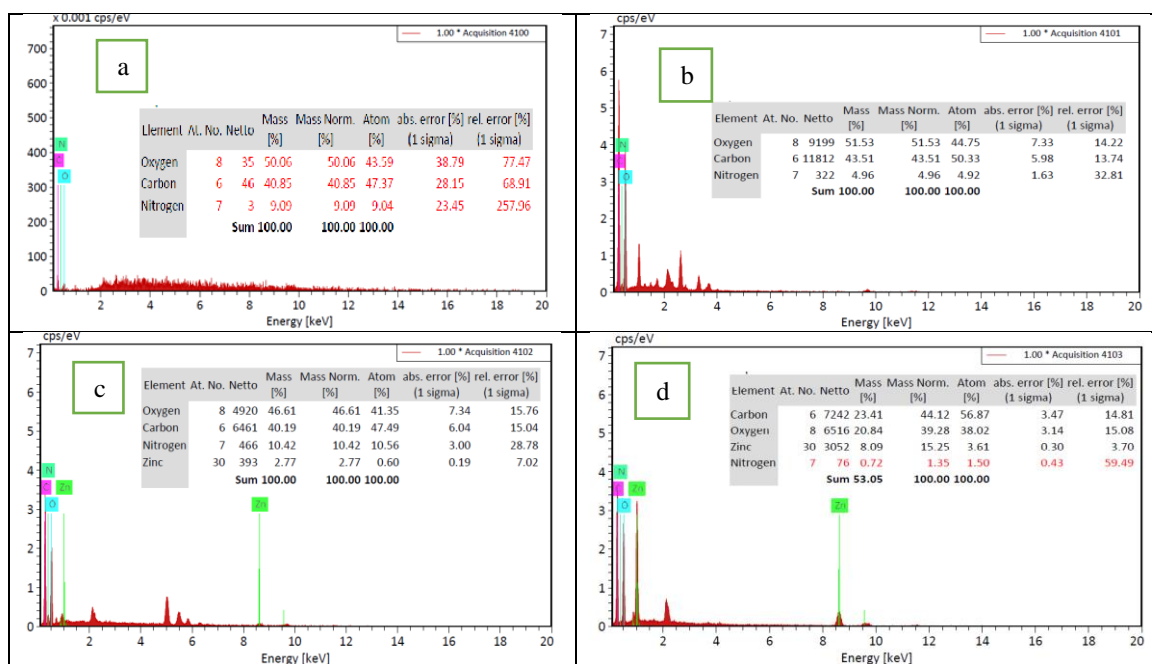


Figure 8: EDX spectrum of (a)chitosan, (b) CSB, (c) Zn (II) @CSB and, (d) ZnO @CSB nanocomposite hydrogels

3.2.5. TEM analysis

The morphology and partial size of the Zn@CSB and ZnO@CSB nanocomposite hydrogels were confirmed by TEM analysis (Fig. 9). Fig. 9a represents the Zn@CSB nanocomposite. The structure exhibited a uniform, aggregated rod-shaped morphology. Fig. 9b illustrates the ZnO@CSB nanocomposite hydrogel with a uniform, spherical morphology.

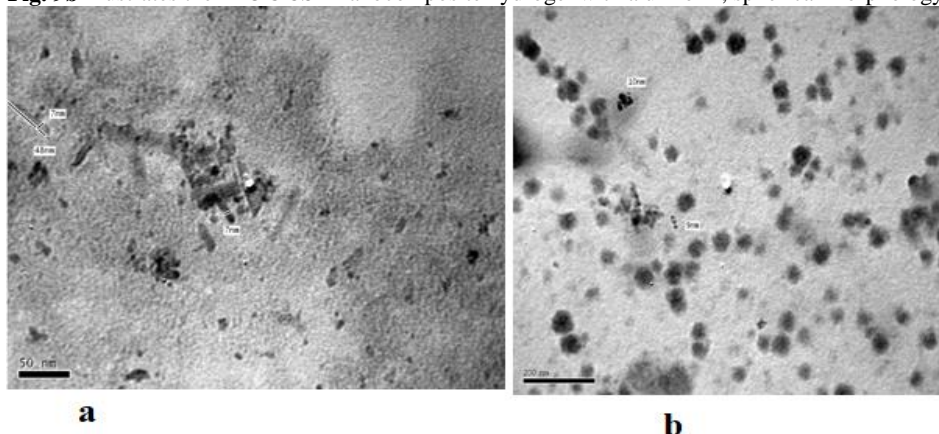


Figure 9: TEM images of (a) Zn(II)@CSB and (b) ZnO@CSB nanocomposite hydrogels

3.2.6. UV-Vis Spectroscopy

The electronic spectra of Chitosan, its CSB hydrogel, Zn(II)@CSB, and ZnO@CSB nanocomposite hydrogels (Fig. 10) in DMSO. The transitions that occurred at wavelengths below 400 nm were determined to be ($\pi \rightarrow \pi^*$) and ($n \rightarrow \pi^*$) intra-ligand charge transfer. Fig. 10 shows that the $n \rightarrow \sigma^*$ transition of amine-free electrons is responsible for the 276 nm absorption bands of chitosan. The CSB exhibited strong absorption bands in regions 255 and 298; these bands were attributed to the aromatic ring's $\pi \rightarrow \pi^*$ and the imine ($-C=N$) $n \rightarrow \pi^*$ electronic transitions, respectively. The new transition band $n \rightarrow \pi^*$ refers to the formation of the azomethine (Schiff base) bond [48]. In the spectra of Zn(II)@CSB and ZnO@CSB hydrogels, the high-intensity bands corresponding to $C=N$ bonds, indicative of $\pi \rightarrow \pi^*$ transitions, are visible, with a blue shift of 291 nm for Zn(II)@CSB and 295 nm for ZnO@CSB. These changes indicate the chemical alteration of the CSB hydrogel by Zn ions and nanoZnO. The lone pairs of electrons on the N atoms interacting with metal ions altered the conjugated structure of the ligand molecule, causing these changes. Furthermore, the appearance of a weak new band at 326 nm refers to the successful formation of nano ZnO [49].

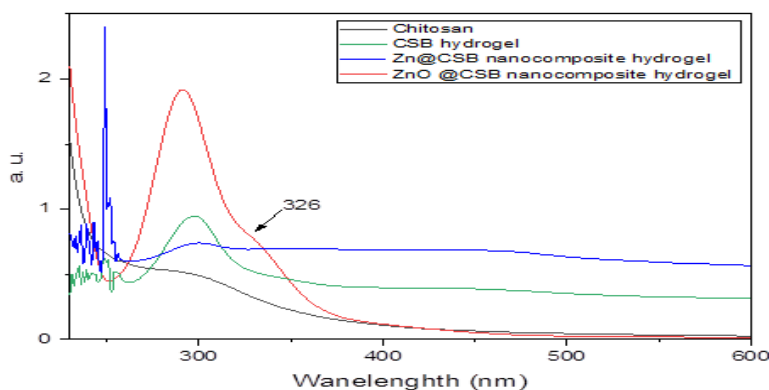


Figure 10: UV-vis spectrum of chitosan and prepared hydrogels

3.2.7 TGA analysis

We used TGA and DTA to examine the thermal stability of the CSB hydrogel and nano-composites. The TGA measures the amount and rate of change in the mass. The thermal behaviour of CS, CSB, and their composites from 25 °C to 600 °C with a heating rate of 10 °C/min in dry air. The results of the TGA and DTA are illustrated in Figs. 11 (a) and 11(b) and Table 1. The chitosan flakes are used as a blank. The chitosan degradation is carried out in three stages, while the degradation of the hydrogel samples is carried out in four steps. The first step of degradation (from room temperature to 120 °C) of chitosan and hydrogel samples is due to the loss of hydrated water dehydration [50]. The 2nd step of CS indicates that it is thermally stable, with no loss. The 2nd step of hydrogel samples CSB (8.4% loss), 1% Zn@CSB hydrogel (7.3% loss), 1.5 % Zn@CSB hydrogel (5% loss), and ZnO@CSB (3.8% loss) owing to loss of physically trapped (H_2O , solvent of the crystal lattice), and nitrate groups in the inner sphere of the metal composite. The 3rd step decomposition of the polymeric chain: chitosan (38.2% loss), CSB (26.9%), 1% Zn@CSB (21.3% loss), 1.5% Zn@CSB (32.3% loss), and ZnO@CSB nanocomposite hydrogel (28.2% loss). The 4th step loss for all samples is greater than 45 % and is attributed to the decomposition of the saccharide ring [51]. As shown in Fig. 11 b, the dehydration step is endothermic, while the other steps are exothermic [45]. The presence of metal in the third step increased the weight loss. The chelation process may alter chitosan's rigidity, leading to changes in its

structure and the formation of new phases. It is illustrated from the TGA analysis that (Fig.11 a), the thermal stability increased in all hydrogel samples except 1.5 % Zn@CSB hydrogel. The unreacted metal ions may cause a decrease in thermal stability in case 1.5% Zn@CSB hydrogel acts as a catalyst [50].

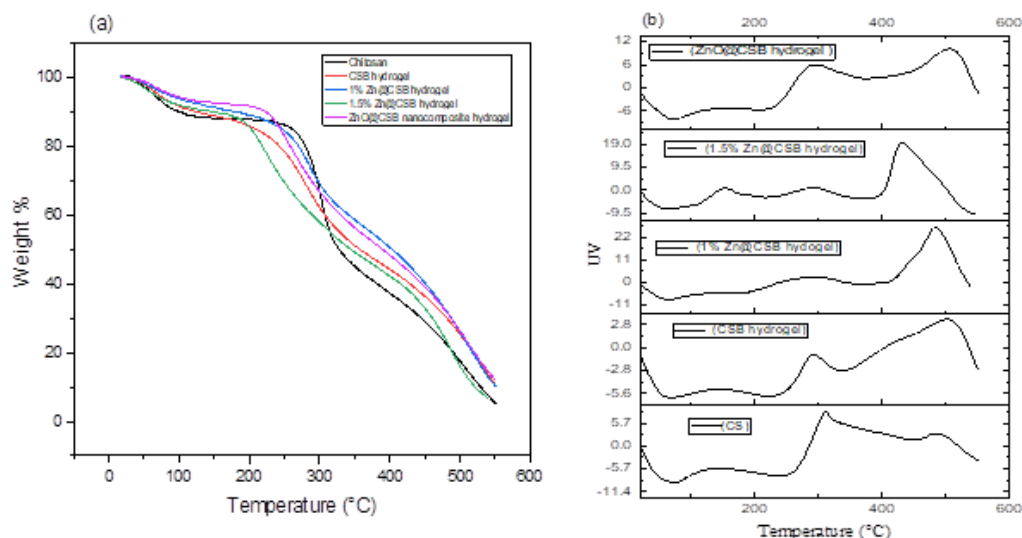


Figure 11: (a) TGA and (b) DTA analysis of prepared hydrogels

Table 1: The mass loss results constructed from thermogravimetric analysis (TGA)

Sample	Temp range (°C)	Mass loss (%)	DTA	Process
Chitosan	21-109	12.5	77(Endo)	Decomposition of the hydrated water
	109-227	0.00	150(Exo)	Thermally stable (mass loss 0%)
	227-319	38.2	305(Exo)	Decomposition of the polymeric chain
	319-550	45.2	480(Exo)	Decomposition of the saccharide rings and
CSB hydrogel	21-118	9.2	72(Endo)	Decomposition of the hydrated water
	118-225	8.4	141(Exo)	Decomposition of trapped solvents and water
	225-320	26.9	290(Exo)	Decomposition of the polymeric chain
	320-550	46	510(Exo)	Decomposition of the saccharide rings and Schiff base
1% Zn@CSB hydrogel	21-112	6.8	63(Endo)	Decomposition of trapped solvents and water
	112-240	7.3	140(Exo)	Decomposition of trapped solvents, water, and loss of nitrate groups
	240-317 317-550	21.3 53	283(Exo) 488(Exo)	Decomposition of the polymeric chain Decomposition of the saccharide rings and Schiff base metal composite
1.5 % Zn@CSB hydrogel	21-91	8	66(Endo)	Decomposition of trapped solvents and water
	91-183	5	153(Exo)	Decomposition of trapped solvents, water, and loss of nitrate groups
	183-314 314-550	32.3 47.8	288(Exo) 433(Exo)	Decomposition of the polymeric chain Decomposition of the saccharide rings and its Schiff base metal composite
ZnO@CSB nanocomposite hydrogel	21-125	7	73(Endo)	Decomposition of trapped solvents and water
	125-223	3.8	147(Exo)	Decomposition of trapped solvents, water, and loss of nitrate groups
	223-325 325-550	28.2 49	291(Exo) 504(Exo)	Decomposition of the polymeric chain Decomposition of the saccharide rings and its Schiff base metal nanocomposite

3.2.8. Antimicrobial activity

The antimicrobial activity of the prepared CSB hydrogels and their modification with Zn(II) ions and ZnO nanoparticles was tested against *S. aureus*, *E. coli*, and *C. albicans* using the disk diffusion method. The antimicrobial test results for CSB (0.5% THB), CSB (1% THB), Zn(II) 1% @CSB, Zn(II) 1.5% @CSB, and ZnO @CSB hydrogels are presented in Fig. 12 and Table 2. As shown in Fig. 12, all hydrogels exhibited inhibitory effects against *S. aureus*, *E. coli*, and *C. albicans*. The diameter of the inhibition zone of the samples against *S. aureus*, *E. coli*, and *C. albicans* was 11–13, 11–16 mm, and 11–19 mm, respectively, revealing that the hydrogels possessed an antibacterial activity that was broad in extent. It was effective for both Gram-negative bacteria, Gram-positive bacteria and fungi. Zn(II) 1% @CSB and Zn(II) 1.5% @CSB hydrogels exhibited higher antimicrobial activity compared to CSB (0.5% THB) and CSB (1% THB), suggesting that the release of Zn metal enhanced the antimicrobial properties of the hydrogels. The mechanism postulated for these nanocomposite hydrogels is that the positively charged Zn(II) ions in the hydrogels can bind to the bacteria's negatively charged cell wall, thereby disrupting the cell wall's structure and releasing the cell's contents. The result of this can be the death of cells or an inhibition of growth [52]. An additional mechanism that has been postulated is that the metal ions in the nanocomposite hydrogels can generate

reactive oxygen species (ROS), which damage the bacterial cell membrane and its components, ultimately leading to cell death. [53-56]. It is worth noting that ZnO@CSB nanocomposite hydrogel displayed a remarkable ability to inhibit the growth of *S. aureus*, *Escherichia coli*, and *C. albicans* in comparison with CSB (0.5% THB), CSB (1% THB), Zn (II) 1% @CSB, Zn (II) 1.5% @CSB hydrogels. The ZnO effect can be discussed into two mechanisms. The first is a photocatalytic antibacterial mechanism; due to its potent photocatalytic properties, nano-zinc oxide exhibits a significant oxidizing capability when exposed to ultraviolet light [57]. The second is metal ion dissolution, which involves ZnO gradually releasing Zn ions into the aqueous media, which can disrupt the structural integrity of membrane proteins [58-59].

Table 2: The antimicrobial activity of the CSB and its composite hydrogels

The prepared hydrogel	The diameter of the inhibition zone (mm/mg Sample)		
	G ⁺	G ⁻	Fungi
	<i>S.aureus</i>	<i>E.coli</i>	<i>C. Albicans</i>
CSB (0.5% THB)	11 ± 0.2	11 ± 0.64	11 ± 1.2
CSB (1% THB)	11 ± 0.34	11 ± 0.41	11 ± 0.81
Zn (II) 1% @CSB	11 ± 0.50	14 ± 0.21	14 ± 1.32
Zn (II) 1.5% @CSB	12 ± 1.2	14 ± 0.35	15 ± 0.72
ZnO @CSB	13 ± 0.57	16 ± 0.47	19 ± 0.23

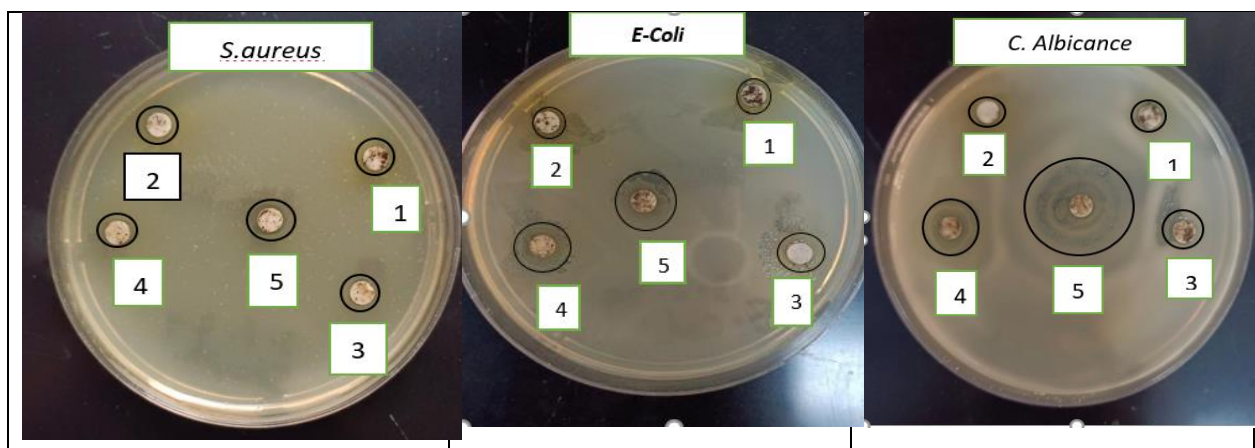


Figure 12 : Inhibitory effect of (1) CSB (0.5% THB), (2) CSB (1% THB), (3) Zn (II) 1% @CSB, (4) Zn (II) 1.5% @CSB, and (5) ZnO @CSB hydrogels

3.2.9. Mechanical properties (tensile strength and elongation at break)

Table 3 summarises the findings of the tensile strength and elongation at break tests. As shown in Table 3, the tensile strength and elongation at break were enhanced from 59.5 MPa to 63.76 MPa and from 8.3% to 7.01%, respectively, by increasing the concentration of crosslinking from CSB 0.5% THB to CSB 1% THB. This may be due to the formation of a chemical bond, or linkage, between the NH₂ group of chitosan and the CHO group of THB. After adding Zn(II), there was a remarkable increase in the tensile strength value, reaching 72.62%. This suggests the coordination covalent bond of Zn ions has a positive effect on the mechanical properties of CSB hydrogel. Compared to Zn(II), the ZnO@CSB nanocomposite hydrogel exhibits the highest values of tensile strength and elongation at break. This could be because the attachment of nano zinc oxide crystals to the hydrogel surface may enhance its mechanical properties.

Table 3: Mechanical properties of the prepared hydrogels

Prepared hydrogels	Tensile Strength (MPa)	Elongation at Break (%)
CSB (0.5% THB)	59.5 ± 0.54	8.3 ± 0.52
CSB (1% THB)	63.76 ± 0.91	7.01 ± 0.45
Zn (II) 1% @CSB	70.94 ± 1.01	6.43 ± 1.32
Zn (II) 1.5% @CSB	72.62 ± 0.72	6.02 ± 1.27
ZnO @CSB	79.43 ± 0.64	5.34 ± 0.80

4. Conclusion

In conclusion, novel hydrogels were effectively created by cross-linking chitosan with Schiff base binding in varying ratios. We subsequently synthesised a nanocomposite of these hydrogels with Zn(II) and nano ZnO. NMR, FTIR, XRD, and UV-Vis spectrophotometer studies confirmed the presence of functional groups in the CSB hydrogel and its metal nanocomposite.

TEM analysis reveals the formation of hydrogels in rod and spherical forms for Zn(II)@CSB and ZnO@CSB nanocomposite hydrogels. SEM results showed rough surfaces with different porous structures for the neat hydrogel and its Zn and ZnO nanocomposites. TGA confirmed that the CSB hydrogel and its nanocomposite were thermally stable. Adding more crosslinker to the CSB hydrogel reduces its swelling degree. Results illustrated that 0.5 % of THB and 45°C represent the optimum conditions for preparing hydrogels. The prepared hydrogels exhibited pH-dependent swelling characteristics. Antimicrobial analysis revealed that the all-prepared hydrogels exhibited antimicrobial activity against *S. aureus*, *E. coli*, and *C. albicans*, making them suitable for drug delivery and wound dressing applications. Moreover, all prepared hydrogels have exhibited good mechanical properties. In general, ZnO@CSB nanocomposite hydrogels are expected to be promising antimicrobial candidates in medical applications.

5. Conflicts of interest

No conflicts of interest.

6. Acknowledgements: “The authors gratefully acknowledge Qassim University, represented by the Deanship of Scientific Research, on the financial support for this research under the number (2023-SDG-1-BSRC36938) during the academic year 1445 AH / 2023 AD”

7. References

1. Mallick, S. P., Suman, D. K., Singh, B. N., Srivastava, P., Siddiqui, N., Yella, V. R., Madhual, A., & Vemuri, P. K., Strategies toward development of biodegradable hydrogels for biomedical applications. *polymer-plastics technology and materials*, 2020, 59(9), 911–927.
2. M. Zhang, M. Yang, M.W. Woo, Y. Li, W. Han, X. Dang, High-mechanical strength carboxymethyl chitosan-based hydrogel film for antibacterial wound dressing, *Carbohydrate Polymers*, 2021, 256, p. 117590.
3. Ali H, Ismail AM. Recyclable and biodegradable Ag@chitosan nanocomposite beads synthesized in one-step for catalytic hydrogenation of 4-Nitrophenol. *J Polym Environ* 2022; 30: 3379–3390.
4. Woźniak, A., & Biernat, M. Methods for crosslinking and stabilization of chitosan structures for potential medical applications. *Journal of Bioactive and Compatible Polymers*, 2022, 37(3), 151-167..
5. Tamer, T. M., Hassan, M. A., Omer, A. M., Baset, W. M., Hassan, M. E., El-Shafeey, M. E., & Eldin, M. S. M. Synthesis, characterization and antimicrobial evaluation of two aromatic chitosan Schiff base derivatives. *Process Biochemistry*, 2016, 51(10), 1721-1730.
6. Zargar, V., Asghari, M., & Dashti, A. A review on chitin and chitosan polymers: structure, chemistry, solubility, derivatives, and applications. *ChemBioEng reviews*, 2015, 2(3), 204-226.
7. Ehterami, A., Rezaei Kolarijani, N., Nazarnezhad, S., Alizadeh, M., Masoudi, A., & Salehi, M. Peripheral nerve regeneration by thiolated chitosan hydrogel containing taurine: in vitro and in vivo study. *Journal of Bioactive and Compatible Polymers*, 2022, 37(2), 85-97.
8. Zheng, X., Zheng, H., Xiong, Z., Zhao, R., Liu, Y., Zhao, C., & Zheng, C. Novel anionic polyacrylamide-modify-chitosan magnetic composite nanoparticles with excellent adsorption capacity for cationic dyes and pH-independent adsorption capability for metal ions. *Chemical Engineering Journal*, 2020, 392, 123706.
9. Eid, M., & Yehia, R. Swelling modelling and kinetics investigation of polymer hydrogel composed of Chitosan-g-(AA-AM). *Egyptian Journal of Chemistry*, 2021, 64(10), 5999-6005..
10. Salama, H. E., Saad, G. R., & Sabaa, M. W. Synthesis, characterization and biological activity of Schiff bases based on chitosan and arylpyrazole moiety. *International journal of biological macromolecules*, 2015, 79, 996-1003.
11. Mcyotto, F., Wei, Q., Macharia, D. K., Huang, M., Shen, C., & Chow, C. W. Effect of dye structure on color removal efficiency by coagulation. *Chemical Engineering Journal*, 2021, 405, 126674.
12. El-Gendy, A. A., Abou-Yousef, H., Adel, A. M., & El-Shinnawy, N. Bio-based hydrogel formed by gamma irradiation. *Egyptian Journal of Chemistry*, 2016, 59(4), 647-662.
13. Varma, A. J., Deshpande, S. V., & Kennedy, J. F. Metal complexation by chitosan and its derivatives: a review. *Carbohydrate polymers*, 2004, 55(1), 77-93.
14. Youssef, F., Mohamed, G., Ismail, S., Elzorba, H., Galal, A., & Elbanna, H. Synthesis, characterization and in vitro antimicrobial activity of florfenicol-chitosan nanocomposite. *Egyptian journal of chemistry*, 2021, 64(2), 941-948.
15. Wang, Y. A., Liu, T., & Zhong, G. Q. Synthesis, characterization and applications of copper (II) complexes with Schiff bases derived from chitooligosaccharide and iodinated salicylaldehyde. *Carbohydrate Polymers*, 2019, 224, 115151.
16. Xu, J. X., Lin, Y. T., Lin, Q., Yuan, W., Yin, X. Q., & Cao, Y. . Preparation, characterization and antibacterial activity of chitosan schiffbases. *Advanced Materials Research*, 2011, 287, 1947-1951.
17. Emam, H. E., & Shaheen, T. I. Design of a dual pH and temperature responsive hydrogel based on esterified cellulose nanocrystals for potential drug release. *Carbohydrate Polymers*, 2022, 278, 118925..
18. Ahmed, H. B., Emam, H. E., & Shaheen, T. I. Fluorescent antimicrobial hydrogel based on fluorophore N-doped carbon dots originated from cellulose nanocrystals. *Scientific Reports*, 2024, 14(1), 29226.
19. Shi, J., Guobao, W., Chen, H., Zhong, W., Qiu, X., & Xing, M. M. Schiff based injectable hydrogel for in situ pH-triggered delivery of doxorubicin for breast tumor treatment. *Polymer Chemistry*, 2014, 5(21), 6180-6189.
20. Xin, Y., & Yuan, J. Schiff's base as a stimuli-responsive linker in polymer chemistry. *Polymer Chemistry*, 2012, 3(11), 3045-3055.

21. Abd El-Hady, M. M., Farouk, A., Saeed, S. E. S., & Zaghoul, S. Antibacterial and UV protection properties of modified cotton fabric using a Curcumin/TiO₂ nanocomposite for medical textile applications. *Polymers*, 2021, 13(22), 4027.
22. Wang, Y., Luo, Q., Sun, R., Zha, G., Li, X., Shen, Z., & Zhu, W. Acid-triggered drug release from micelles based on amphiphilic oligo (ethylene glycol)-doxorubicin alternative copolymers. *Journal of Materials Chemistry B*, 2014, 2(43), 7612-7619.
23. Xu, H., & Matysiak, S. Effect of pH on chitosan hydrogel polymer network structure. *Chemical Communications*, 2017, 53(53), 7373-7376.
24. Abdalla, T. H., Nasr, A. S., Bassioni, G., Harding, D. R., & Kandile, N. G. Fabrication of sustainable hydrogels-based chitosan Schiff base and their potential applications. *Arabian Journal of Chemistry*, 2022, 15(1), 103511.
25. Xu, C., Zhan, W., Tang, X., Mo, F., Fu, L., & Lin, B. Self-healing chitosan/vanillin hydrogels based on Schiff-base bond/hydrogen bond hybrid linkages. *Polymer testing*, 2018, 66, 155-163.
26. Heydari, N., Karimi, A. R., Momeni, H. R., Azadikhah, F., & Etemadi, T. Chitosan Schiff-Base Hydrogel Sunscreen: A Multifunctional Hybrid Network with Antioxidant, Ultraviolet-Shielding, and Self-Healing Properties. *ACS omega* 2025.
27. Zhang, M., Qiao, X., Han, W., Jiang, T., Liu, F., & Zhao, X. Alginate-chitosan oligosaccharide-ZnO composite hydrogel for accelerating wound healing. *Carbohydrate polymers*, 2021, 266, 118100.
28. Liao, C., Li, Y., & Tjong, S. C. Bactericidal and cytotoxic properties of silver nanoparticles. *International Journal of Molecular Sciences*, 2019, 20 (2), 449.
29. Alavi, M., & Nokhodchi, A. An overview on antimicrobial and wound healing properties of ZnO nanobiofilms, hydrogels, and bionanocomposites based on cellulose, chitosan, and alginate polymers. *Carbohydrate Polymers*, 2020, 227, 115349.
30. He, X., Liu, R., Liu, H., Wang, R., Xi, Z., Lin, Y., et al. Facile preparation of tunicate-inspired chitosan hydrogel adhesive with self-healing and antibacterial properties. *Polym. (Basel)* 2021, 13, 4322.
31. CLSI, Methods for Dilution Antimicrobial Susceptibility Tests for Bacteria That Grow Aerobically; Approved Standard—Ninth Edition, Vol. 32 No. 2, M07-A9 Clinical and Laboratory Standards Institute USA, 2012.
32. Xu, C.; Zhan, W.; Tang, X.; Mo, F.; Fu, L.; Lin, B. Self-Healing Chitosan/Vanillin Hydrogels Based on Schiff-Base Bond/ Hydrogen Bond Hybrid Linkages. *Polym. Testing*, 2018, 66, 163.
33. Bi, X., & Liang, A. In situ-forming cross-linking hydrogel systems: chemistry and biomedical applications. *Emerging concepts in analysis and applications of hydrogels*, 2016, 86, 541-547.
34. Saeed, S. E. S., Al-Harbi, T. M., Alhakimi, A. N., & Abd El-Hady, M. M. Synthesis and characterization of metal complexes based on aniline derivative Schiff base for antimicrobial applications and UV protection of a modified cotton fabric. *Coatings*, 2022, 12(8), 1181.
35. Karimi, A. R., Rostaminejad, B., Rahimi, L., Khodadadi, A., Khanmohammadi, H., & Shahriari, A. Chitosan hydrogels cross-linked with tris (2-(2-formylphenoxy) ethyl) amine: Swelling and drug delivery. *International journal of biological macromolecules*, 2018, 118, 1863-1870.
36. Ebrahimi, R. The study of factors affecting the swelling of ultrasound-prepared hydrogel. *Polymer Bulletin*, 2019, 76(2), 1023-1039.
37. Khorasani, M. T., Joorabloo, A., Moghaddam, A., Shamsi, H., & Mansoori Moghadam, Z. Incorporation of ZnO nanoparticles into heparinized polyvinyl alcohol/chitosan hydrogels for wound dressing application. *International journal of biological macromolecules*, 2018, 114, 1203-1215.
38. Maity, S., Naskar, N., Jana, B., Lahiri, S., & Ganguly, J. Fabrication of thiophene-chitosan hydrogel-trap for efficient immobilization of mercury (II) from aqueous environs. *Carbohydrate Polymers*, 2021, 251, 116999.
39. Ahmed, M., Omer., Abdelazeem, S., Eltaweil., Esmail, M., El-Fakharany., Eman, M., Abd, El-Monaem., Magda, M., F., Ismail., Mohamed, S., Mohy-Eldin., Mohammed, Salah, Ayoup. Novel Cytocompatible Chitosan Schiff Base Derivative as a Potent Antibacterial, Antidiabetic, and Anticancer Agent. *Arabian journal for science and engineering*, 2023, 48(6):1-15.
40. Brugnerotto, J., Lizardi, J., Goycoolea, F. M., Arguelles-Monal, W., Desbrières, J., & Rinaudo, M. An infrared investigation in relation to chitin and chitosan characterization. *Polymer*, 2001, 42(8), 3569-3580.
41. Barbosa, H.F.G.; Attjioui, M.; Ferreira, A.P.G.; Dockal, E.R.; El Gueddari, N.E.; Moerschbacher, B.M.; Cavaleiro, É.T.G. Synthesis, Characterization and Biological Activities of Biopolymeric Schiff Bases Prepared with Chitosan and Salicylaldehydes and Their Pd(II) and Pt(II) Complexes. *Molecules* 2017, 22, 1987.
42. Iftime, M. M., Morariu, S., & Marin, L. Salicyl-imine-chitosan hydrogels: Supramolecular architecturing as a crosslinking method toward multifunctional hydrogels. *Carbohydrate Polymers*, 2017, 165, 39-50.
43. Juneja, H. D., Joshi, M., & Kanfode, J. P. Synthesis and characterization of metallic gel complexes derived from carboxymethyl cellulose. *Journal of Chemistry*, 2013, 2013(1), 820328.
44. Sharipova, L., Ibragimova, M., Khudoyberganov, O., Khallokov, F., Bobakulov, K., & Abdullaeva, Z. Synthesis and study of the complex compound of isonicotinamide with zinc nitrate. *The Eurasia Proceedings of Science Technology Engineering and Mathematics*, 2024, 30, 47-55.
45. Rajalakshmi, A., Krithiga, N., & Jayachitra, A. J. M. E. J. S. R. (). Antioxidant activity of the chitosan extracted from shrimp exoskeleton. *Middle East J. Sci. Res*, 2013, 16(10), 1446-1451.

46. Saif, M., El-Shafiy, H. F., Mashaly, M. M., Eid, M. F., Nabeel, A. I., & Fouad, R. Synthesis, characterization, and antioxidant/cytotoxic activity of new chromone Schiff base nano-complexes of Zn (II), Cu (II), Ni (II) and Co (II), *Journal of Molecular Structure*, 2016, 1118: 75-82.
47. Kai, J., & Xuesong, Z. Preparation, characterization, and cytotoxicity evaluation of zinc oxide–bacterial cellulose–chitosan hydrogels for antibacterial dressing. *Macromolecular Chemistry and Physics*, 2020, 221(21), 2000257..
48. Barbosa, H. F. G., Attjioui, M., Ferreira, A. P. G., Dockal, E. R., El Gueddari, N. E., Moerschbacher, B. M., & Cavalheiro, É. T. G. Synthesis, characterization and biological activities of biopolymeric schiff bases prepared with chitosan and salicylaldehydes and their Pd (II) and Pt (II) complexes. *Molecules*, 2017, 22(11), 1987..
49. Malekshah, Rahime Eshaghi, et al. "Developing a biopolymeric chitosan supported Schiff-base and Cu (II), Ni (II) and Zn (II) complexes and biological evaluation as pro-drug." *International journal of biological macromolecules* 152 (2020): 846-861.
50. Malekshah, R. E., Shakeri, F., Khaleghian, A., & Salehi, M. Developing a biopolymeric chitosan supported Schiff-base and Cu (II), Ni (II) and Zn (II) complexes and biological evaluation as pro-drug. *International journal of biological macromolecules*, 2020, 152: 846-861
51. 46. Matar, G. H., Kaymazlar, E., Andac, M., & Andac, O. Novel Binary Blended Hydrogel Films (Chitosan-Vanillin Schiff Base/Locust Bean Gum and Fe (III), Cu (II) & Zn (II) Complexes): Synthesis, Characterization, Conductivity, and Antibacterial Activity. *Journal of Polymers and the Environment*, 2023, 31.8: 3509-3521
52. El-Sayed Saeed, S., Al-Harbi, T. M., Abdel-Mottaleb, M. S., Al-Hakimi, A. N., Albadria, A. E., & Abd El-Hady, M. M.. Novel Schiff base transition metal complexes for imparting UV protecting and antibacterial cellulose fabric: Experimental and computational investigations. *Applied Organometallic Chemistry*, 2022, 36(12), e6889.
53. Guarnieri, A., Triunfo, M., Scieuzo, C., Ianniciello, D., Tafi, E., Hahn, T., ... & Falabella, P. Antimicrobial properties of chitosan from different developmental stages of the bioconverter insect *Hermetia illucens*. *Scientific Reports*, 2022,12(1), 8084.
54. Saeed, S., Alomari, B. A., Alhakimi, A. N., El-Hady, A., Alnawmasi, J. S., Elganzory, H. H., & El-Sayed, W. A. Pyrimidine hydrazide ligand and its metal complexes: synthesis, characterization, and antimicrobial activities. *Egyptian Journal of Chemistry*, 2023, 66(5), 315-329.
55. Saeed, S. E. S., Aldubayyan, M., Al-Hakimi, A. N., El-Sayed, W. A., Alnawmasi, J. S., El-Hady, M. M. A., & Abdel-Mottaleb, M. S. A. . UV protective textile: Experimental and DFT computational studies on the function of some metal complexes of hydrazide derivatives on cellulose fabrics. *Applied Organometallic Chemistry*, 2023, 37(8), e7140.
56. Abou Zeid, S., Perez, A., Bastide, S., Le Pivert, M., Rossano, S., Remita, H., & Leprince-Wang, Y. Antibacterial and photocatalytic properties of ZnO nanostructure decorated coatings. *Coatings*, 2023, 14(1), 41.
57. Saeed, S. E. S., Aldubayyan, M., Al-Hakimi, A. N., & El-Hady, M. M. A.. Synthesis and Characterization of Pyridine Acetohydrazide Derivative for Antimicrobial Cotton Fabric. *Materials*, 2023,16(13), 4885.
58. Kai, J., & Xuesong, Z. Preparation, characterization, and cytotoxicity evaluation of zinc oxide–bacterial cellulose–chitosan hydrogels for antibacterial dressing. *Macromolecular Chemistry and Physics*, 2020, 221(21), 2000257.
59. Saeed, S. E. S., Alomari, B. A., Abd El-Hady, M. M., & Al-Hakimi, A. N. Novel Pyrimidinethione Hydrazide Divalent and Trivalent Metal Complexes for Improved High-Performance Antimicrobial and Durable UV Blocking Cellulosic Fabric. *Inorganics*, 2023, 11(6), 231.